

Analysis of orthogonal matching pursuit based subsurface imaging for compressive ground penetrating radars

Mehmet Ali Çağrı TUNCER, Ali Cafer GÜRBÜZ*

*Department of Electric and Electronics Engineering,
TOBB University of Economics and Technology, Ankara-TURKEY
Söğütözü Cad. No 43, Ankara-TURKEY
e-mail: matuncer@etu.edu.tr, acgurbuz@etu.edu.tr*

Received: 04.04.2011

Abstract

It is shown that compressive sensing (CS) theory can be used for subsurface imaging in stepped frequency ground penetrating radars (GPR), resulting in robust sparse images, using fewer measurements. Although the data acquisition time is decreased by CS, the computational complexity of the minimization based imaging algorithm is too costly, which makes the algorithm useless, especially for extensive discretization or 3D imaging. In this paper, a greedy alternative, orthogonal matching pursuit (OMP) is used for imaging subsurface and its performance under various conditions is compared to CS imaging method. Results show that OMP could reconstruct sparse signals robustly as well as CS imaging. It is faster and easier to implement so it can be said that OMP is a fascinating alternative to CS imaging method for subsurface GPR imaging.

Key Words: *Ground Penetrating Radar (GPR), Radar, Subsurface Imaging, Compressive Sensing (CS), ℓ_1 minimization, Orthogonal Matching Pursuit (OMP)*

1. Introduction

Ground Penetrating Radar (GPR) is an important nondestructive remote sensing tool which images the subsurface by transmitting short electromagnetic pulses into the ground then receiving the reflections [1, 2, 3, 4]. Since GPRs can detect anything presenting electromagnetic contrast, such as variation in permittivity, relative to the surrounding medium, they are used in a wide variety of areas such as landmine detection [5, 7], through to wall imaging and detection [8, 9] in archeological surveys [10, 11, 12] or other various civil applications [13, 6].

The types of GPR are time, and frequency domain GPRs, related to how the data acquisition is performed. Time domain or impulse, GPR is used widely in commercial systems due to its simple design and low cost [1].

*Corresponding author: Department of Electric and Electronics Engineering, TOBB University of Economics and Technology, Ankara-TURKEY

This work was supported by The Scientific and Technical Research Council of Turkey (TUBITAK) under Career program grant with contract agreement 109E280 and within the Marie Curie IRG Grant with grant agreement PIRG04-GA-2008-239506.

The other type of GPR that is becoming popular is the stepped frequency continuous wave GPR (SFCW-GPR) [14, 15]. This type of GPR transmits a discrete set of frequencies to and through the medium and constructs imaging using the reflections and their phase differences.

SFCW-GPR has several advantages over an impulse GPR, such as greater measurement accuracy, greater dynamic range and lower noise. In addition, the operating frequency range can be adaptively adjusted for targets at different depths, or be programmed to skip over a defined frequency band, so instruments on sensitive bands will not interfere with SFCW-GPR. Although this is an advantageous property of SFCW-GPR, time at each scan position and at each frequency takes much more time in total compared to impulse GPR systems [16, 17, 18].

The advent of works on decreasing the data acquisition time have been introduced in the literature [19, 20, 21]. These recent methods exploit the theory of compressive sensing (CS) [22, 23, 24]. It assumes the sparsity of target space, which is a general reasonable assumption since the potential targets cover a small part of the total subsurface volume to be imaged. It is shown in CS theory that a sparse signal $x = \Psi s$ can be reconstructed using small number of linear measurements $y = \Phi x$ in the form of randomized projections by solving a constraint ℓ_1 minimization problem which can be solved using linear programming. In [19, 20, 21], the target space is discretized and a GPR data dictionary is formed by modeling the data expected to be acquired for each discrete target location. Hence a linear relation is formed between measurements and the target space. Later, an ℓ_1 minimization based optimization problem constraint to the measurements is solved.

The target space can be constructed using smaller number of random frequency step measurements and random spatial positions as shown in [19]. Considering the results, less cluttered images compared to standard back-projection methods are obtained using fewer number of frequency measurements. The CS method in [19] also provides super resolution property and robust to noise and random spatial sampling. In practical SFCW-GPRs, CS imaging method decreases the data acquisition time.

Despite these efforts, successful results have been presented for CS imaging; yet the effect of time spent for target space reconstruction has not been considered. Candes and Le Bret in [23, 25] show the computational cost of CS imaging increases with N^3 , where N is the total discrete points of the target space. That means that, although CS reduces the data acquisition time, it spends too much time in image reconstruction which makes the algorithm useless for real time applications, especially for high discretization or 3D imaging.

The formulated dictionary selection problem in [19] could also be solved using the Basis Pursuit algorithms [26, 27, 28, 29]. These methods, which obtain sparse solutions, are principally iterative greedy algorithms and they do not guarantee any global optimum solution as in [19]. But, they are computationally very efficient.

In this paper, a robust greedy method, orthogonal matching pursuit (OMP) [28, 29] is used for subsurface imaging and its performance is compared against the method of compressive sensing (CS) to show that it can be a viable alternative. In addition, range gain is added to OMP reconstruction procedure which allows one to image targets with their correct RCS values. Hence the proposed method could also image deep targets that were lost in the standard CS reconstruction in [19]. For comparison purposes, fewer measurements are taken instead of measuring all frequencies; and when the measurement number is more than one tenth of the all frequencies, OMP could exactly reconstruct the sparse signal with similar performance as CS. Also, effects of signal-to-noise ratio (SNR) on OMP and CS imaging methods are investigated. It is observed that these two methods show similar reconstruction performances when the SNR is more than 10 dB. OMP and CS methods are applied to 20 independent simulated data sets on the same computer and the average time spent found in CS method is 497.341 seconds, while the OMP method took only 0.897 seconds. This means that OMP is practical for larger area imaging, higher discretization or a 3D area imaging, where CS is not. In brief, this

work shows that OMP is faster than the CS method and it could reconstruct sparse signals robustly as well as CS imaging. Thus, it is more implementable than CS imaging method in real systems. With the proposed method, while systems could decrease their data acquisition times through fewer measurements, the processing time would be decreased by OMP without important performance degradation compared to ℓ_1 minimization.

Remainder of this paper is organized as follows. Section 2 briefly describes the compressive subsurface imaging algorithm for stepped frequency GPRs. The proposed fast subsurface imaging method using OMP is explained in Section 3. Section 4 presents the CS and OMP based imaging and comparison results for imaging performance, noise and computational complexity and experimental GPR data results. Conclusions are drawn in Section 5.

2. Compressive imaging for SF-GPR

In this section a brief summary of CS based subsurface imaging developed in [19, 20, 21] is given. A SF-GPR transmits L continuous sinusoidal signals during scan of a region. In [19], the transmitted signal for frequency ℓ is shown as

$$E_T(\ell, t) = Ae^{-j2\pi(f_0 + \ell\Delta f)t} = Ae^{-j\omega_\ell t}, \quad (1)$$

where $\omega_\ell = 2\pi(f_0 + \ell\Delta f)$, f_0 is the initial frequency, $\ell = 0, 1, 2, \dots, L-1$ with the total number of frequency steps L , and Δf is the frequency step interval. A is the strength of the transmitted signal. Assuming the scanned medium is homogeneous and its parameters are known, for a bistatic GPR sensor, the received signal for a single point target at position p when the GPR is at the scan position i can be written as

$$E_R(\ell, t, p, i) = \alpha(p)e^{j(k_1 r_1 + k_2 r_2 - \omega_\ell t)}, \quad (2)$$

where the distances depend on p and i , $\alpha(p) = A\sigma/S(R(p))$, σ is the reflection coefficient of the target, $S(R)$ is the spreading function explaining the decay of the signal, k_1 and k_2 are the propagation constants in air and soil, r_1 and r_2 are total travel distances of signal in air and soil, respectively. Also, equation (2) can be written in terms of the total time delay as $\tau_i(p) = r_1/v_1 + r_2/v_2$; and v_1 and v_2 are the propagation velocities in air and soil, respectively.

The sparsity assumption is that the targets cover only a small portion of the whole target space, which is generally fair. To be able to use any prior information about target space, such as sparsity, the measurements must be related linearly to the spatial domain image:

$$d(u_x, u_y, f) = \Psi \pi_T(x, y, z), \quad (3)$$

where $d(u_x, u_y, f)$ is the space frequency measurements, $\pi_T(x, y, z)$ is the target space and Ψ is the operator defining the transform between two spaces.

The target space, which is in the $[x_i, x_f] \times [y_i, y_f] \times [z_i, z_f]$, must be discretized to create the forward model Ψ . (x_i, y_i, z_i) and (x_f, y_f, z_f) denotes the target space's initial and final positions to be imaged. Discretization generates $\mathcal{B} = \{\pi_1, \pi_2, \dots, \pi_N\}$, where N denotes the resolution and each π_j is a 3D vector $[x_j; y_j; z_j]$. The points π_j are candidate discrete points at target positions. At any discrete target position, the received frequency data for each frequency step and for each scan position can be calculated using (2), with $\alpha(\pi_j) = 1/R_j^2$, R_j being the distance to the target point π_j . For a target at π_j and the GPR at the i^{th}

scan position, the j^{th} column of Ψ_i can be written as

$$[\Psi_i]_j = \alpha(\pi_j) \exp[-j\omega(t - \tau_i(\pi_j))], \tag{4}$$

where ω is the vector of L frequencies. For P targets, measurements of the frequency response at the i^{th} scan position can be written as

$$\zeta_i(\omega) = \sum_{k=1}^P \mathbf{b}(\mathbf{k}) \exp[-j\omega(t - \tau_i(\pi_k))] = \Psi_i \mathbf{b}. \tag{5}$$

Our goal is to find weighted indicator \mathbf{b} , which is actually an image of the medium.

In [19], a random subset of $M < L$ frequencies are measured instead of measuring all L frequency steps at each scan position, then the new measurements β_i can be shown as

$$\beta_i = \Phi_i \zeta_i = \Phi_i \Psi_i \mathbf{b}, \tag{6}$$

where Φ_i is an $M \times L$ measurement matrix constructed by randomly selecting M rows of an $L \times L$ identity matrix. This reduces the data acquisition time by a factor of L/M .

It is shown in [30, 31, 32, 33] that stable recovery of the vector \mathbf{b} is possible by solving the modified convex optimization problem:

$$\hat{\mathbf{b}} = \arg \min \|\mathbf{b}\|_1 \quad \text{such that} \quad \|\mathbf{A}^T(\beta - \mathbf{A}\mathbf{b})\|_\infty < \epsilon_1, \tag{7}$$

where $\mathbf{A} = \Phi \Psi$. The optimization problems in (7) minimize convex functionals, so a global optimum is guaranteed for CS.

3. Fast subsurface imaging with OMP

In [19], the image vector \mathbf{b} using the measurements β_i is obtained through solving convex ℓ_1 minimization problem shown in equation (7). For optimizing (7), the complexity increases as N^3 , where N denotes the total discrete points of the target space [23, 25]. That means although CS imaging method reduces the data acquisition time, image reconstruction takes too much time because of convex optimization programming. For larger area imaging, finer grid sizes or 3D imaging, this becomes an important problem that makes the algorithm unusable. Therefore, to reduce the computational complexity and to utilize a more implementable algorithm for fast subsurface imaging, a suboptimal solver, orthogonal matching pursuit [28, 29] is used. Although OMP does not guarantee any global optimal solution, it is computationally very efficient. It is shown that it could reconstruct sparse signals robustly. For a system like $y = Ax + n$, the iterative algorithm applied is as follows:

- 1) Initialize the index set $\Lambda_0 = \emptyset$. The residual $r_0 = y$ and the loop index to $t = 1$.
- 2) Find an index $\lambda_t \in \arg \max_w |\langle r_{t-1}, A_w \rangle|$ where A_w are columns of \mathbf{A} .
- 3) Update the index sets $\Lambda_t \leftarrow \Lambda_{t-1} \cup \lambda_t$.
- 4) Determine the weights \mathbf{c} of the best least squares problem $\min \left\| y - \sum_{k=1}^t c(\Lambda_t) A_{\lambda_k} \right\|_2$.
- 5) Compute the new residual using the least square weights \mathbf{c} : $r_t = y - \sum_{k=1}^t c(\Lambda_t) \varphi_{\lambda_k}$.
- 6) Increment the loop counter: $t \leftarrow t + 1$.

7) Until the stop criterion has been met, return to Step 2, otherwise terminate iteration.

Conditions similar to those used by equation (7) can be selected to cease the iteration. For stop criteria, a threshold can be set conditional on the estimated noise level or the original data norm, such as $0.1 \|y\|_2$. When the norm of the residual \mathbf{r} drops below the determined threshold, the iteration can be terminated. Similar methods are also shown as stopping criteria in [28, 29].

4. Results

For subsurface imaging with SF-GPR, several simulations are presented in this section. To exemplify the random frequency sampling idea, a 2D homogeneous target space of size $30 \text{ cm} \times 30 \text{ cm}$ is created. A bistatic antenna with a 5 cm transmitter-receiver spacing at a height of 10 cm is simulated to collect frequency domain measurements between 100 MHz and 10 GHz with 100 MHz step size resulting in 100 frequency measurements at each scan point if all frequencies are measured. An antenna beamwidth of 40° is assumed. The radiated power is assumed to be equal over the beamwidth and no power is assumed to be radiated outside of the antenna beamwidth. True target space which contains five randomly placed targets modeled as point reflectors can be seen in Figure 1(a). The SNR for simulation is 10 dB. When all the space-frequency domain data is measured and frequency domain back-projection (BP) [34, 35, 36] is applied, Figure 1(b) is obtained, where the five targets can be seen at the correct target positions.

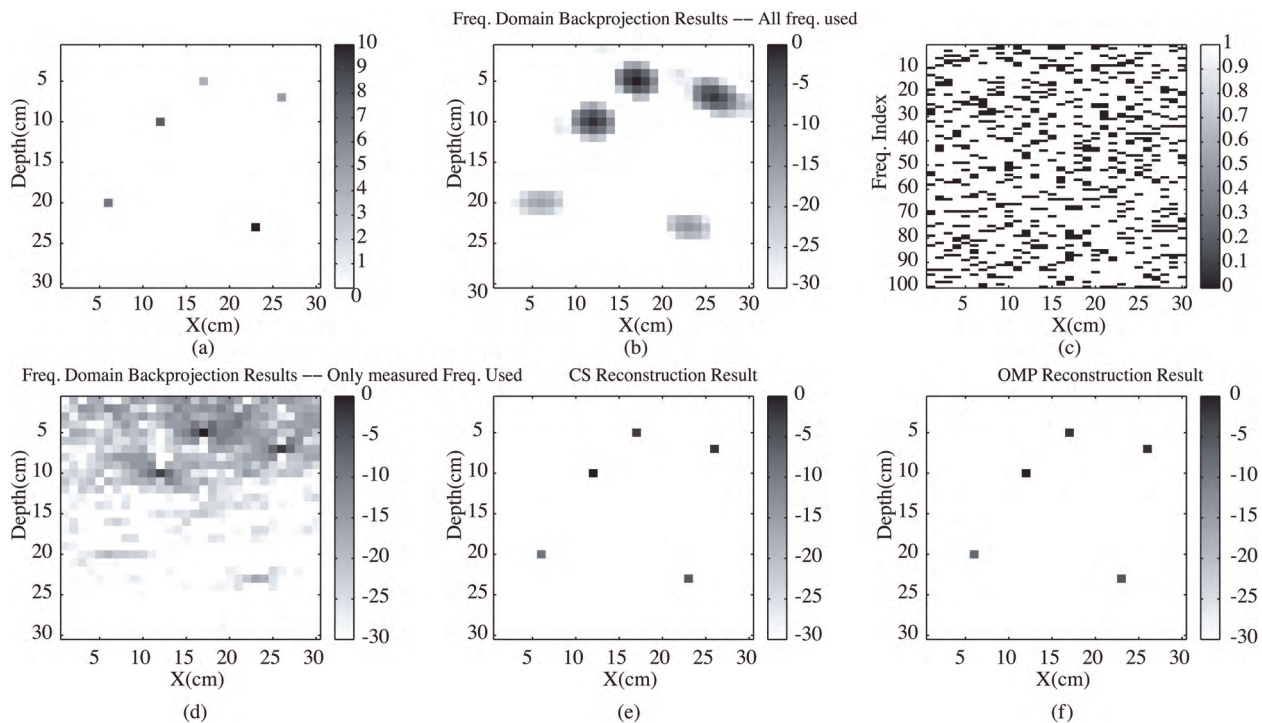


Figure 1. Plots showing (a) the True Target Space; (b) Imaging with the BP method using all frequencies; (c) Randomly measured frequencies, using frequencies in (b); (d) Imaging with the BP method; (e) Imaging with the CS method; and (f) Imaging with OMP

Considering the CS imaging theory developed in [19], instead of measuring all 100 frequencies, only a random subset of 20 frequencies at each scan position, shown in Figure 1(c), is measured. If frequency domain BP is applied to the randomly selected data, the degraded imaging result is shown in Figure 1(d). In order to obtain CS imaging, solving (7) with the randomly measured frequencies shown in Figure 1(c) obtains Figure 1(e). As seen, CS method could generate a less cluttered image that is better than the BP method, using all the frequency data or randomly measured small number of frequencies. If the same randomly measured frequencies are applied to OMP method, the resulting image is shown in Figure 1(f). The results show that OMP and CS imaging methods give similar images and they find the correct target positions with less clutter than the BP method. In addition, adding range gain into the image reconstruction procedure helped both CS and OMP to recover deeper targets with more correct RCS values. Overall this simulation shows OMP can be a good alternative to CS, but imaging performance and computational complexity of both algorithms should be compared in detail. Next subsections show these comparisons.

4.1. Comparison of computational complexity

In Figure 1, OMP and CS methods show similar imaging performances. Nevertheless, to understand the actual computational performance differences between OMP and CS methods, more detailed simulations were done in which time spent for image reconstruction is compared among the methods. Increasing the grid target space step-by-step from 100 to 1225 grids, the image is 20 times formed independently by selecting 10 and 50 independent random measurements at each time step and, respectively, applying OMP and CS methods. Result of these simulations are shown in Figure 2, which shows average execution times of OMP and CS methods on logarithmic scale as a function of target space. Note that the computation time of the OMP method is many times smaller than the computation time of CS. Computation time for both methods grow with target space size; from first order polynomial fit, the growth rate for CS is $O(N^{3.17})$ and the computation time for OMP grows at a rate of only $O(N^{1.6})$. Hence, the computational time difference becomes more influential as the target space grows. This is a very important property of OMP that makes it a good candidate algorithm for

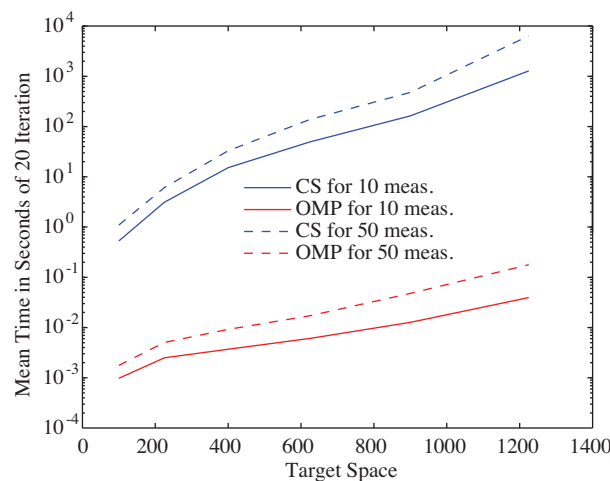


Figure 2. Graph of execution times for image reconstruction, in logarithmic scale as a function of normalized average error.

imaging larger target spaces or 3D subsurface imaging. Figure 2 also shows that the computational complexity mainly depends on the target size, not the number of measurements taken at each scan position. Although an increase in the measurement number increases slightly the time spent for reconstructing the image, its effect is smaller compared to the effect of target space N .

4.2. Analysis on measurement and sparsity level

Although OMP requires less execution time for reconstruction, it does not guarantee a global solution. Thus new simulations were performed to compare the correct reconstruction performances of OMP and CS methods. OMP and CS methods are applied to different data sets having frequency measurement numbers between 1 and 50, acquired from $20\text{ cm} \times 20\text{ cm}$ scanned area, on which 1, 3, and 10 target groups were randomly placed; each simulation repeated 100 times.

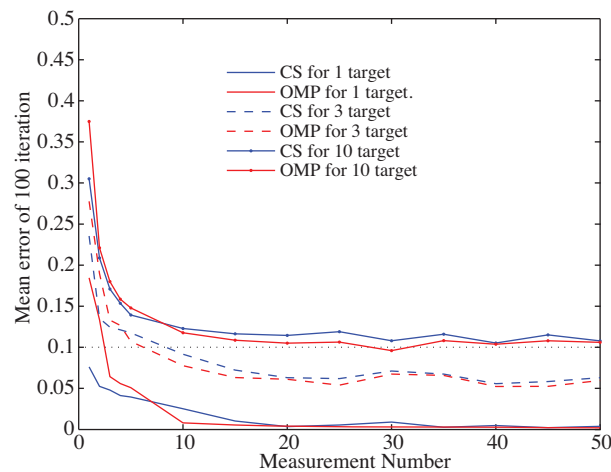


Figure 3. Graph of measurement number as a function of normalized average error.

To calculate the error between the correct target space and the reconstructed image the average error values, representing incorrect reconstruction, are normalized with the norm of the target spaces, to realize reconstruction performances of both methods, with varying number of targets and/or with different number of measurements. The obtained results are shown in Figure 3. The graph clearly demonstrates that if the measurement number is more than 10, one tenth of the all frequency measurement number 100, OMP and CS methods can reconstruct the image successfully with similar error values. Also it is seen that as the target number is increasing, the correct reconstruction performances of both methods are decreasing likely. For very less number of measurements both methods fail to reconstruct the target spaces correctly.

4.3. Noise analysis

We turn now to the effect of noise on the OMP reconstruction, and analysis of the CS method. For this, individual simulations were done with 10 and 20 measurements for $20\text{ cm} \times 20\text{ cm}$ scanned regions with 1 cm discretization level where a 3 point target is randomly localized. Figure 4 shows the normalized average reconstruction error versus SNR level, computed over 100 trials.

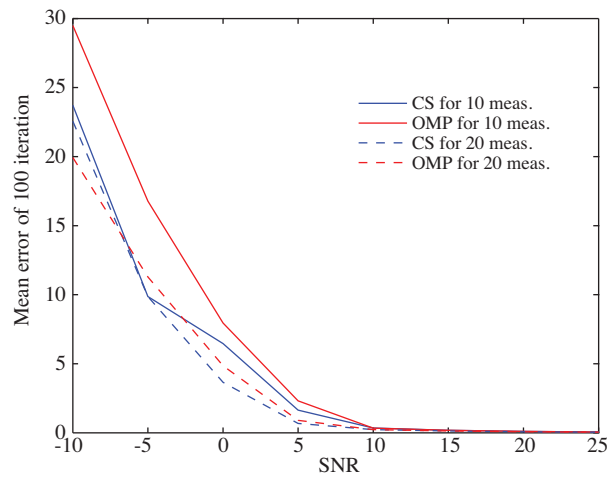


Figure 4. Plot of SNR versus normalized average error, computed over 100 trials.

As observed in Figure 4, if the SNR is more than 10 dB, OMP is as successful as the CS method in reconstructing the images. For very low SNR, CS shows slightly better performance compared to OMP. Results on all simulated data show that as OMP can as well reconstruct the image in comparison as the CS method, with much lower computational cost, which makes it faster and more implementable for large regions or 3D imaging, and it works with similar correct reconstruction performances.

4.4. Experimental data results

CS and OMP methods are applied to experimental SF-GPR data obtained from [37, 38, 39]. The GPR is scanned over a 1.8 m × 1.8 m, mostly homogeneous, dry sand region from 27.8 cm height above a nearly flat surface with 2 cm increments in x and y directions. 401 equally spaced frequency measurements from 60 MHz to 8.06 GHz are collected using a multistatic array over a buried scenario. Data is used from a single bistatic pair, and one slice of that 3D data is used. The time domain representation of the data is given in Figure 5(a). There are two shallow and one deep targets at $x = \{-40, +5, +50\}$ cm, respectively. Their presence are

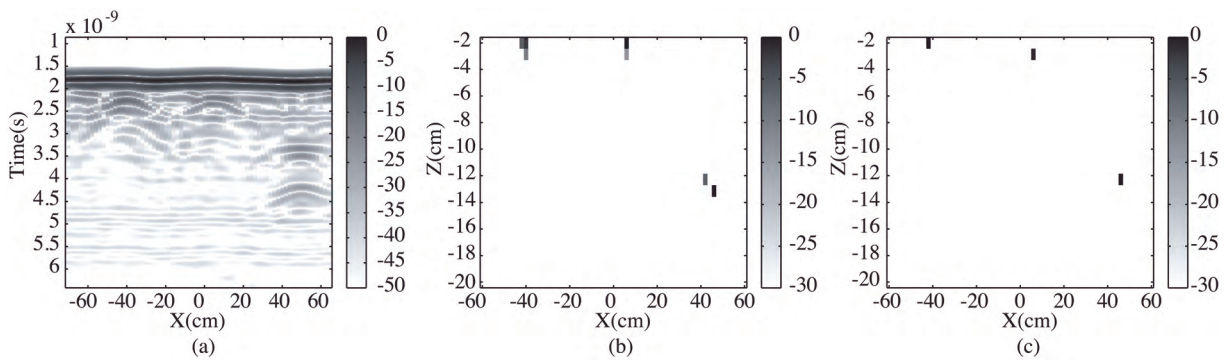


Figure 5. (a) Space-time domain representation with all frequencies measured; (b) CS based imaging result; and (c) OMP based imaging result

seen clearly from the time domain data. For sparse imaging, CS and OMP methods are applied to only 200 randomly selected frequency measurements at each scan position, instead of using all 401 measurements. The resulting images of both methods are shown in Figure 5(b) and Figure 5(c), respectively. The results show that OMP can successfully reconstruct the real data images as the CS imaging method. In addition, while CS takes 24.411 seconds to reconstruct, OMP method takes only 0.156 seconds to generate its result. CS seems to reconstruct more detail about the target scene compared to OMP, but both methods successfully finds all the targets.

5. Conclusions

In this work, simulations were done to compare the performances of Orthogonal Matching Pursuit (OMP) and Compressive Sensing (CS) methods. For a more correct comparison, OMP and CS methods are improved by adding range gain; hence targets are detected with their correct RCS values and this increases the detection probability of deep targets. OMP has much less computational complexity than CS and simulations showed that increase in the computational complexity with grid size is also significantly reduced with OMP. Results show that OMP, with measurements over fewer frequencies, can exactly reconstruct the sparse signals with performance similar to CS. Both methods show similar reconstruction performance against different signal-to-noise ratios (SNR). OMP is faster and easier to implement, and provides other performances similar to CS. Hence, OMP can be a fascinating alternative to CS imaging method for subsurface imaging.

References

- [1] D. Daniels, *Ground Penetrating Radar*, 2nd ed. London, U.K., The Inst.Elect.Eng.(IEE), 2004.
- [2] H. M. Jol, *Ground Penetrating Radar: Theory and applications*, Elsevier, 2009.
- [3] L. Sevgi, Modeling and simulation strategies in high frequency surface wave radars, *Turk. J. Elec. Eng. and Comp. Sci.*, 18, (2010), 399–408.
- [4] G. Apaydın, L. Sevgi, Propagation modeling and path loss prediction tools for high frequency surface wave radars, *Turk. J. Elec. Eng. and Comp. Sci.*, 18, (2010), 469–484.
- [5] J. Groenenboom, A. Yaravoy, Data processing and imaging in GPR system dedicated for landmine detection, *Subsurf. Sens. Technol.*
- [6] A. C. Gurbuz, Line detection with adaptive random samples, *Turk. J. Elec. Eng. and Comp. Sci.*, 19, (2011), 21–32.
- [7] P. Gader, M. Mystkowski, Y. Zhao, Landmine detection with ground penetrating radar using hidden Markov models, *IEEE Trans. Geosci. Remote Sens.*, vol. 39, pp. 1231–1244, 2001.
- [8] E. J. Baranoski, Through-wall imaging: Historical perspective and future directions, *Journal of the Franklin Institute* 345, pp. 556–569, 2008
- [9] N. Metje, et.al., Mapping the underworld-state of the art review, *Tunnel. Underground Space Technol.*, vol.22, pp. 568–586,2007.
- [10] S. Hubbard, C. Jinsong, K. Williams, Y. Rubin, J. Peterson, Environmental and agricultural applications of GPR, in *Proc. 3rd Int. Workshop on Adv. Ground Penetrating Radar*, 2005, pp. 45–49

- [11] M. Sciotti, F. Colone, D. Pastina, T. Bucciarelli, GPR for archaeological investigations: Real performance assessment for different surface and subsurface conditions, in Proc. IGARSS 03, 2003, pp. 2266–2268
- [12] A. C. Gurbuz, J. H. McClellan, W. R. Scott, Seismic tunnel imaging and detection, IEEE International Conference on Image Processing (ICIP 2006), pp. 3229–3232, 2006
- [13] G. Grandjean, J. Gourry, A. Bitri, Evaluation of GPR techniques for civil-engineering applications: Study on a test site, *J. Appl. Geophys.*, vol. 45, no. 3, pp. 141–156, 2000.
- [14] A. Langman, The design and hardware and signal processing for a stepped frequency continuous wave ground penetrating radar, Phd thesis, University of Cape Town, 2002
- [15] K. Iizuka, A.P. Freundorfer, K.H. Wu, H. Mori, H. Ogura, V-K. Nguyen, 1984, Step-frequency radar. *Journal Applied Physics*, Vol 56, pp. 2572–2583.
- [16] F. Kong, T. L. By, performance of a GPR system which uses step frequency signals, *J. Appl. Geophys.*, vol. 33, pp. 15–26, 1995
- [17] W. Steinway, C. Barret, Development status of a stepped-frequency ground penetrating radar, in Proc. SPIE, 1993, vol. 1942, pp.34–43
- [18] M. Bradley, T. Witten, R. Mccummins, M. Crowe, S. Stewart, M. Duncan, Mine detection with a multi-channel stepped-frequency ground penetrating radar, in Proc. SPIE, 1999, vol 3710, pp. 953–960.
- [19] A.C. Gurbuz, J.H. McClellan, W.R. Scott, A Compressive Sensing Data Acquisition and Imaging Method for Stepped-Frequency GPRs, *IEEE Tran. On Signal Processing*, Vol. 57(7), July 2009, pp. 2640–2650
- [20] A.C. Gurbuz, J. H. McClellan, W.R. Scott, Compressive Sensing for Subsurface Imaging using Ground Penetration Radar, *Signal Processing*, Vol. 89(10), October 2009, Pages:1959–1972
- [21] A.C. Gurbuz, J. H. McClellan, W. R. Scott, Jr., Compressive Sensing for GPR Imaging, 41st Asimolar Conference on Signals, Systems and Computers, November 2007.
- [22] D. Donoho, Compressed sensing, *IEEE Trans. Inf. Theory*, vol. 52, no. 4, pp. 1289–1306, 2006
- [23] E. Candes, J. Romberg, T. Tao, Robust uncertainty principles: Exact signal reconstruction from highly incomplete frequency information, *IEEE Trans. Inf. Theory*, vol.52, pp. 489–509, 2006.
- [24] R. Baraniuk, Compressive sensing, *IEEE Signal Process. Mag.*, vol. 24, no. 4, pp. 118–121, Jul. 2007
- [25] S. Boyd, L. Vandenberghe, *Convex Optimization*. Cambridge, U.K.; Cambridge Univ. Press, 2004
- [26] S.S. Chen, D. L. Donoho, M. A Saunders, Atomic decomposition by basis pursuit, *SIAM J. Sci. Comput.*, vol 20, pp. 33–61, 1999.
- [27] S. Mallat, Z. Zhang, Matching pursuits with time-frequency dictionaries, *IEEE Trans. Signal Process.*, vol. 41, pp. 3397–3415, Dec. 1993
- [28] J. Tropp, A. Gilbert, Signal recovery from random measurements via orthogonal matching pursuit, *IEEE Trans. Information Theory*, vol. 53, no. 12, pp.4655–4666 Dec. 2007
- [29] H. Krim, M. Viberg, Signal Recovery From Random Measurements via Orthogonal Matching Pursuit, *IEEE Trans. on Info. Theory* 53(12): 4655–4666, 2007.

- [30] E. Candes, J. Romberg, T. Tao, Stable signal recovery from incomplete and inaccurate measurements, *Comm. Pure Appl. Math.*, vol. 59, no. 8, pp. 1207–1223, 2006.
- [31] E. Candes, T. Tao, The Dantzig selector: Statistical estimation when p is much larger than n , *Ann. Statist.*, vol. 35, no. 6, pp. 2313–2351, 2007
- [32] J. Haupt, R. Nowak, Signal reconstruction from noisy random projections, *IEEE Trans. Inf. Theory*, vol. 52, no. 9, pp. 4036–4048, 2006
- [33] D. Donoho, M. Elad, V. Temlyakov, Stable recovery of sparse overcomplete representations in the presence of noise, *IEEE Trans. Inf. Theory*, vol. 52, no: 1, pp. 6–18, 2006
- [34] J. Gazdag, Wave equation migration with the phase shift method, *Geophys.*, vol. 43, pp. 1342–1351
- [35] R. Stolt, Migration by Fourier transform, *Geophys.*, vol. 43, pp. 23–48, 1978
- [36] W. Schneider, Integral formulation of migration in 2 and 3 dimensions, *Geophys.*, vol.43, pp. 49–76, 1978
- [37] W.R.Scott, <http://users.ece.gatech.edu/wrscott/>
- [38] T. Counts, A.C. Gurbuz and W.R. Scott, Jr. and J. H. McClellan and K. Kangwook, Multistatic Ground-Penetrating Radar Experiments, *IEEE Trans. Geoscience and Remote Sensing*, vol. 45, no:8, pp.2544–2553, Aug. 2007.
- [39] K. Kim, A.C. Gurbuz, WR. Scott, et al, A multi-static ground-penetrating radar with an array of resistively-loaded vee dipole antennas for landmine detection, *Conference on Detection and Remediation Technologies for Mines and Minelike Targets X*, vol. 5794, pp.495–506, Mar. 28–April 01, 2005, Orlando, FL.